Retinal degeneration depends on Bmi1 function and reactivation of cell cycle proteins

Dusan Zencak[a], Karine Schouwey[a,1], Danian Chen[b,1,2], Per Ekström[c], Ellen Tanger[d], Rod Bremner[b], Maarten van Lohuizen[d], and Yvan Arsenijevic[a,3]

[a]Unit of Gene Therapy and Stem Cell Biology, Jules-Gonin Eye Hospital, University of Lausanne, 1004 Lausanne, Switzerland; [b]Toronto Western Research Institute, University Health Network, Samuel Lunenfeld Research Institute, University of Toronto, Toronto, ON, Canada M5T 2S8; [c]Division of Ophthalmology, Department of Clinical Sciences, Lund University, SE-221 84 Lund, Sweden; and [d]Division of Molecular Genetics and The Centre of Biomedical Genetics, 1066 CX, Amsterdam, The Netherlands

Edited by Ching-Hwa Sung, Weill Medical College of Cornell University, New York, NY, and accepted by the Editorial Board December 26, 2012 (received for review June 9, 2011)

The epigenetic regulator Bmi1 controls proliferation in many organs. Reexpression of cell cycle proteins such as cyclin-dependent kinases (CDKs) is a hallmark of neuronal apoptosis in neurodegenerative diseases. Here we address the potential role of Bmi1 as a key regulator of cell cycle proteins during neuronal apoptosis. We show that several cell cycle proteins are expressed in different models of retinal degeneration and required in the *Rd1* photoreceptor death process. Deleting E2f1, a downstream target of CDKs, provided temporary protection in *Rd1* mice. Most importantly, genetic ablation of *Bmi1* provided extensive photoreceptor survival and improvement of retinal function in *Rd1* mice, mediated by a decrease in cell cycle markers and regulators independent of $p16^{Ink4a}$ and $p19^{Arf}$. These data reveal that Bmi1 controls the cell cycle-related death process, highlighting this pathway as a promising therapeutic target for neuroprotection in retinal dystrophies.

blindness | neurodegeneration | polycomb

Retinitis pigmentosa (RP) is a group of genetic disorders known as a major cause of inherited blindness that is currently untreatable and affects millions of patients worldwide. Around 200 different mutated loci or genes cause this disease (1) (also https://sph.uth.edu/RetNet/sum-dis.htm). *Rd1* mice, a widely used model of RP, carry a mutation in the rod-specific *Phosphodiesterase-6β* (*Pde6b*) gene, which is also mutated in around 4–5% of human RP patients in the United States (1). *Rd1* mice exhibit a rapid loss of rod photoreceptors, which are responsible for night vision, followed by a more gradual loss of cones, which are necessary for day vision and visual acuity. Several studies have attempted to rescue or delay retinal degeneration in *Rd1* mice with neurotrophic factors (2), calcium blockers (3), or anti-apoptotic gene transfer (4), but these neuroprotective approaches never exceeded modest or temporary effects. Interestingly, deleting cyclic nucleotide channel-b1 (CNGB1), which is constantly stimulated by the accumulation of cyclic GMP (cGMP) in *Rd1* photoreceptors, leads to a marked rescue of the sensory cells (5). Because an elevated level of cGMP is believed to be an early event in the induction of cell death in this model, these results can be considered as a milestone reference to conduct the identification of other candidates involved in the photoreceptor death process.

Various models of neurodegenerative diseases have shown that neurons committed to death reexpress cell cycle-related proteins. This phenomenon has been observed in mouse models of Alzheimer's disease (6, 7), Parkinson disease (8), and amyotrophic lateral sclerosis (9), where postmitotic neurons start to express nuclear cyclin-dependent kinase 4 (CDK4), implicated in the reentry into the cell cycle and in the transition from G1 to S phase. However, these cells fail to complete S phase and undergo apoptosis (reviewed in ref. 10). Using CDK inhibitors, interference with CDKs in vitro enhances the survival of motoneurons (11) and sympathetic neurons (12) after trophic factor withdrawal, but these effects remain modest. CDK inhibition before induction of stroke in vivo protects around 80% of neurons (13). However, such success has not been achieved in other types of neuronal degeneration.

At early stages of retinal degeneration in *Rd1* mice, the synthetic thymidine analog Bromodeoxyuridine (BrdU) is incorporated in the outer nuclear layer (ONL) where photoreceptors reside, but this BrdU incorporation has been attributed to DNA repair (14). Nevertheless, DNA replication does occur in neurons of an Alzheimer's disease model (7) as well as in dopaminergic neurons of a patient with Parkinson disease (8), showing that neurons synthesize de novo DNA in an S-like phase. In view of the interesting observations made in animal models and in patient samples of neurodegenerative disorders, we asked whether retinal degeneration is also linked to cell cycle proteins and machinery and tested the potential role of cell cycle regulators in photoreceptor cell death.

During retinogenesis, cell cycle arrest is controlled by a panel of factors, among which the Rb/E2F pathway plays a central role. For example, in the developing retina, retinoblastoma protein (Rb) is required to couple terminal differentiation to cell cycle exit, and thus its absence leads to E2F1-dependent ectopic division (15). In dividing cells, Rb is inactivated by CDK4- or CDK6-mediated phosphorylation, which inhibits its binding to E2F1 (reviewed in ref. 16). Upstream of this pathway, the polycomb group protein Bmi1 promotes CDK4 and CDK6 activity by repressing the *Ink4a/Arf* locus, encoding the CDK4/6 inhibitor $p16^{Ink4a}$ and $p19^{Arf}$ that activates p53 (17). Because the Rb/E2F1 pathway partially contributes to neuronal death in Parkinson disease (8), we investigated whether Bmi1 and E2F1 are required to promote photoreceptor death during retinal degeneration.

Results

Expression of Cell Cycle Proteins in Degenerating *Rd1* Retinas. We analyzed the expression of cell cycle markers in *Rd1* mice at early stages of photoreceptor loss. At postnatal day 9 (P9), when the first apoptotic cells were detected, CDK4 was present in few cells

Author contributions: D.Z., K.S., D.C., P.E., R.B., M.v.L., and Y.A. designed research; D.Z., K.S., D.C., P.E., and E.T. performed research; M.v.L. contributed new reagents/analytic tools; D.Z., K.S., D.C., P.E., R.B., M.v.L., and Y.A. analyzed data; and D.Z., K.S., R.B., and Y.A. wrote the paper.

The authors declare no conflict of interest.

This article is a PNAS Direct Submission. C.-H.S. is a guest editor invited by the Editorial Board.

Freely available online through the PNAS open access option.

[1]K.S. and D.C. contributed equally to this work.

[2]Present address: Department of Ophthalmology, Ophthalmic Laboratory of Molecular Medicine Research Center, and Torsten-Wiesel Research Institute of World Eye Organization, West China Hospital, Sichuan University, Chengdu 610041, China.

[3]To whom correspondence should be addressed. E-mail: yvan.arsenijevic@fa2.ch.

This article contains supporting information online at www.pnas.org/lookup/suppl/doi:10.1073/pnas.1108297110/-/DCSupplemental.

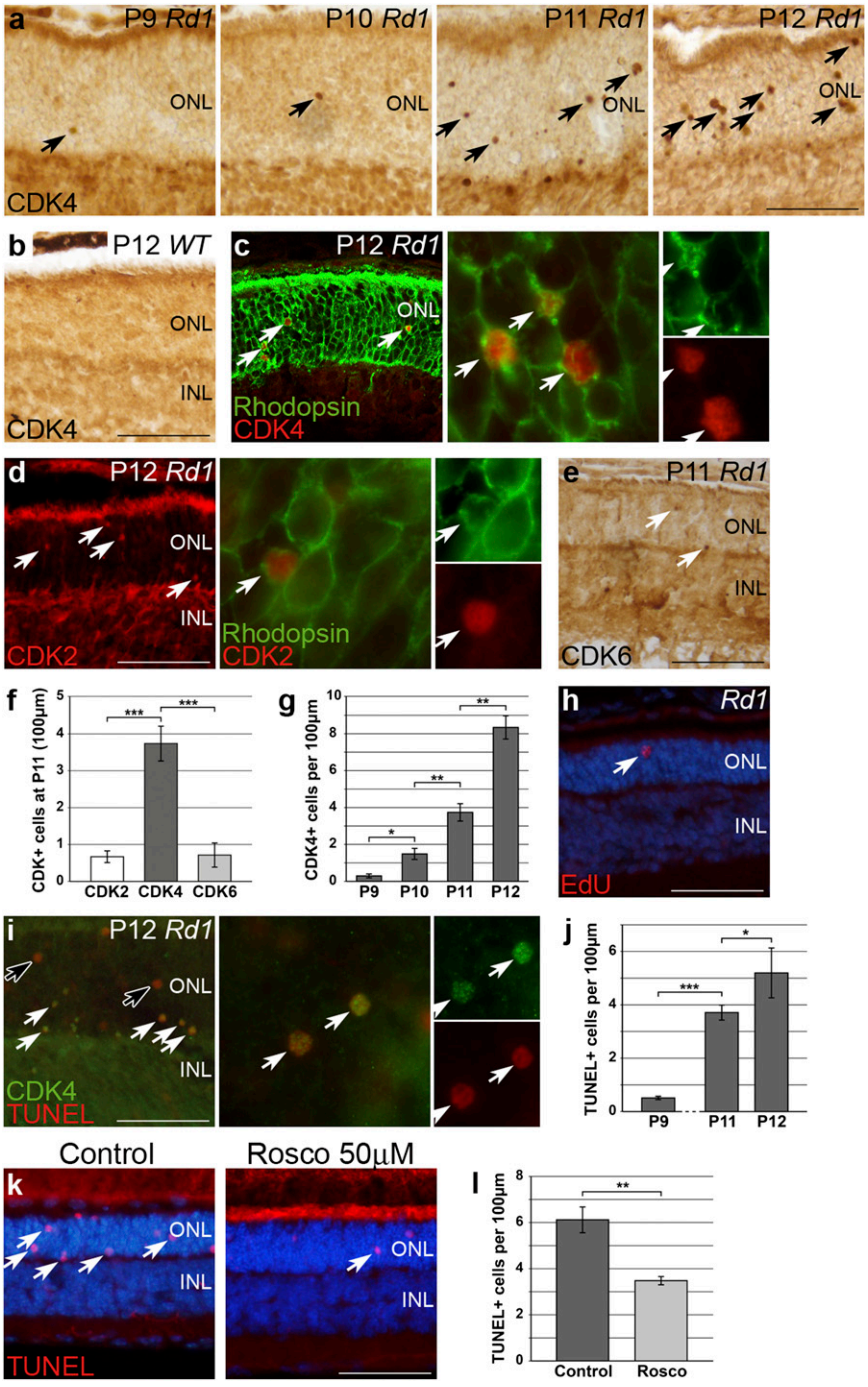

Fig. 1. Cell cycle proteins are expressed in the *Rd1* retina. (*A* and *B*) The *Rd1* retina contains CDK4-expressing cells in the ONL (brown nuclei highlighted by arrows) (*A*), whereas CDK4 is not expressed in WT ONL (*B*). (*C*) At P12, double labeling for CDK4 (red) and Rhodopsin (green) clearly shows that photoreceptor cells express CDK4 in *Rd1* retina (confocal image and enlargement). Arrows point to some representative cells positive for CDK4. (*D*) CDK2 is expressed in sparse *Rd1* photoreceptor nuclei (red, arrows) at P12, evidenced by localization of $CDK2^+$ nuclei rhodopsin-positive cells (green). (*E*) Similarly, CDK6-positive nuclei are detected in the P11 *Rd1* retina (arrows). (*F*) The quantification of CDK-positive nuclei at P11 shows that *Rd1* photoreceptors express CDK4 to a greater extent (more than fivefold) than CDK2 and CDK6. The graph represents the number of CDK-expressing cells in the ONL of central retina ± SEM ($n = 4$ for CDK4, $n = 3$ for CDK2 and CDK6, $^{**}P < 0.01$). (*G*) From their appearance at P9, the number of CDK4-positive nuclei increases with age (P10–P12). The graph represents the mean value of positive cell number in the ONL for each age ± SEM ($n = 5$ at P9, 6 at P11, and 2 at P12, $^{*}P < 0.05$, $^{**}P < 0.01$). (*H*) Rare EdU (red)-positive cells are present in *Rd1* ONL nuclei after a 24-h pulse in *Rd1* mice at P12. A representative labeling is marked by an arrow. (*I*) Most CDK4-expressing photoreceptor cells in the *Rd1* ONL at P11 are dying (TUNEL, red) and CDK4 (green) double-positive cells (arrows). Nevertheless, some single-positive cells can also be detected (open arrows). (*J*) Quantification of TUNEL-positive cells in the *Rd1* central retina shows a gradual increase from P9 to P12 (for TUNEL, $n = 2$ at P9, 6 at P11, and 3 at P12, $^{*}P < 0.05$, $^{***}P < 0.001$) correlating with CDK4 expression (*G*). (*K*) Decreased cell death, as revealed by TUNEL (red), in roscovitine-treated (*Right*) vs. control (*Left*) *Rd1* retinal explants at P6 + 6 DIV ($n = 6$ control and 9 treated *Rd1* explants spread over three series of experiments). (*L*) Quantification of TUNEL+ cells in roscovitine- vs. control-treated *Rd1* explants. Data are expressed as mean ± SEM ($^{**}P < 0.01$). INL, inner nuclear layer; ONL, outer nuclear layer. (Scale bars: 50 µm.)

of the ONL, and then the number of CDK4-positive photoreceptors markedly increased until P12 (Fig. 1 *A–C* and *G*), during the peak of cell death in this model. Quantification revealed that the amount of CDK4-expressing cells doubled between P10 and P11, as well as between P11 and P12 (Fig. 1*G*) in the *Rd1* ONL, whereas almost no CDK4-positive cells were detected in the wild-type (WT) retina (Fig. 1*B*). Costaining with Rhodopsin antibodies and subsequent confocal analysis demonstrated that CDK4 was expressed in rod photoreceptors of degenerating *Rd1* retinas (Fig. 1*C* and Fig. S1). Although not expressed in the WT ONL, CDK2 and CDK6 were also present in the mutant ONL, however, to a lesser extent than CDK4 (Fig.1 *D–F*). No variation of CDK4 and CDK6 expression was detected between the *Rd1* and the WT retina by RT-PCR analysis of total mRNA extracts (Fig. S1), suggesting that the positive signal observed in the cell body and processes of other retinal cells masks the variations observed in the ONL. In addition, phosphorylation of Rb, which is the substrate of CDK4 and CDK6, on serine 807 and 811, was increased in the *Rd1* ONL, showing a link with CDK expression (Fig. S1). The specificity of the antibody was checked by Western blot. We used ethynyl deoxyuridine (EdU) incorporation to test the possibility that dying photoreceptors enter S phase. Very few cells in the ONL integrated EdU (Fig. 1*H*), and their number was much lower than that of the CDK4- and TUNEL-positive cells.

We performed a time-course analysis of CDK4 expression and TUNEL staining in the *Rd1* retina to determine how cell cycle protein expression is related to DNA fragmentation. In the *Rd1* ONL at P9, few cells were TUNEL single positive, and we detected only rare TUNEL/CDK4 double-positive cells and no CDK4 single-positive cells (Fig.1 *G* and *J*). In P11 *Rd1* retinas, a large majority of cells in the death process were double positive for TUNEL and CDK4, around 25% were positive only for TUNEL, and we also detected some CDK4 single-positive cells. Colocalization analyses suggest that CDK4 expression is tightly related to late processes of photoreceptor cell death (Fig. 1*I*).

These results are consistent with a previous study reporting BrdU incorporation in degenerating photoreceptors in *Rd1* mice at P15, where it was attributed to DNA repair because of Ligase IV expression in photoreceptors (14). We did not observe any cells positive for the M-phase marker phospho-H3 in the *Rd1* ONL (Fig. S1), suggesting that CDKs and related proteins of the G1 phase may have a role during photoreceptor death, similar to that in other neurodegenerative diseases.

Reexpression of Cell Cycle Proteins Also Occurs in Other Genetic or Acute Models of Retinal Degeneration. To assess whether cell cycle protein reactivation in photoreceptors during retinal degeneration was specific to *Rd1* mice or common to other models, we analyzed the expression of CDKs in four additional genetic or acute models of retinal degeneration. The *Rd10* mouse is another recessive animal model of PDE6β deficiency (missense mutation) exhibiting a delayed rod degeneration, starting around P18 and complete at P30 in our hands. At the time of photoreceptor loss, CDK4 was expressed in photoreceptor nuclei, and the number of CDK4-positve cells increased considerably from P19 to P23 (Fig. S2). We investigated whether mutations inducing a dominant form of RP are also associated with the reactivation of cell cycle proteins during photoreceptor loss. *P23H* and *S334ter* rats bear mutations in the *Rhodopsin* gene. In both cases, the ONL contained many CDK4-positive nuclei (Fig. S2). Moreover, degenerating retinas of *Rd10* mice, as well as *P23H*, and *S334ter* rats showed higher levels of phosphorylated Rb than WT (Fig. S2). Finally, an acute model of retinal degeneration induced by light damage was investigated. We observed intense and widespread nuclear expression of CDK4 and CDK2 in the ONL 36 h after light damage (Fig. S3), when the cell death process reaches its peak (18). Similar to the P12 WT retina (Fig. 1), control adult retinas did not contain any CDK4- or CDK2-positive photoreceptor nuclei (Fig. S3). Thus, we conclude that reactivation of cell cycle proteins is associated with photoreceptor death in five distinct models of retinal degeneration.

Interference with CDK Function Reduces Apoptosis in *Rd1* Retinal Explants. We next aimed to interfere with cell cycle protein reactivation to reveal their roles during retinal degeneration. We focused on the *Rd1* mouse, which is one of the most severe and therapeutically challenging models of retinal degeneration. We isolated P6 *Rd1* retinas and cultured them as retinal explants ex vivo with or without addition of the general CDK inhibitor roscovitine. Retinal explants were exposed to roscovitine (50 μM) at P6 + 1 d in vitro (DIV) (corresponding to P7 in vivo), fixed, and analyzed at P6 + 6 DIV (corresponding to P12 in vivo). We performed a TUNEL staining on treated and control retinal explant sections to analyze the degree of neuroprotection provided by the CDK inhibitor. Roscovitine treatment caused a 42% reduction in the number of apoptotic photoreceptors (Fig. 1 *K* and *L*), thus implying that roscovitine treatment is neuroprotective and that CDK reactivation plays a key role in the photoreceptor death process.

Activating *E2fs* Contribute to Photoreceptor Cell Death in *Rd1* Mice. Consistent with the above data implicating CDK activation in photoreceptor death, phosphorylated Rb was detected in *Rd1* but not in WT ONL (Fig. S1). E2F1 is released and activated upon Rb phosphorylation and is known to contribute to apoptosis in Parkinson disease (8) and stroke (13). Moreover, *Rb* null rod photoreceptors undergo E2F1-dependent apoptosis (15), and either directed expression of *E2f1* in these cells (19) or inhibition of pRb through T-antigen expression also leads to cell death. Thus, we next asked whether E2Fs contribute to *Rd1* photoreceptor degeneration. E2F1 is one of three activating E2Fs that interchangeably drive the cell cycle in fibroblasts (20) and promote division redundantly with N-Myc in retinal progenitors together (21). We therefore analyzed the effect of deleting combinations of all three factors, using germ-line *E2f1* and *E2f2* null alleles and a floxed *E2f3* allele, which was conditionally deleted using a *Cre* transgene expressed in the peripheral retina only (15). In the *Rd1;E2f1*$^{+/+}$*;E2f2*$^{-/-}$*;E2f3*$^{f/f}$*;α-Cre* P18 retina, the absence of E2F2 in the central retina or E2F2 and E2F3 in the periphery had no effect (Fig. 2 *A–C*). In *Rd1;E2f1*$^{+/-}$*;E2f2*$^{-/-}$*;E2f3*$^{f/f}$*;α-Cre* mice, loss of one *E2f1* allele and both *E2f2* alleles did not prevent photoreceptor loss in the central retina (Fig. 2*C*). However, in *Rd1;E2f1*$^{-/-}$*;E2f2*$^{+/-}$*;E2f3*$^{f/f}$*;α-Cre* mice, the absence of two *E2f1* alleles and one *E2f2* allele increased the number of rescued photoreceptor rows 4.7-fold in the central ONL (39% of WT, Fig. 2*C*). These data imply that E2F1 has a greater role in rod photoreceptor death than E2F2. To assess E2F3 function we studied the periphery, where degeneration is delayed relative to the central retina and where the *E2f3* deletion occurs in this model (Fig. 2). In the *Rd1;E2f1*$^{+/-}$*;E2f2*$^{-/-}$*;E2f3*$^{f/f}$*;α-Cre* retina periphery, which lacks one allele of *E2f1* and both alleles of *E2f2* and *E2f3*, ONL rows were increased 1.9-fold, corresponding to 35% of WT retina (Fig. 2). This effect in the *E2f1*$^{+/-}$*;E2f2*$^{-/-}$*;E2f3*$^{-/-}$ periphery was greater than in the central *E2f1*$^{+/-}$*;E2f2*$^{-/-}$ retina, which could reflect a role for E2F3 in rod death or central vs. peripheral differences. Finally, the peripheral retina of *Rd1;E2f1*$^{-/-}$*;E2f2*$^{+/-}$*;E2f3*$^{f/f}$*;α-Cre* showed improved rescue over that seen in the *Rd1;E2f1*$^{+/-}$*;E2f2*$^{-/-}$*;E2f3*$^{f/f}$*;α-Cre* periphery (Fig. 2*C*), confirming that E2F1 is more important than E2F2. *E2f* removal slowed but did not halt photoreceptor death, because at P26, there was no difference in the central or peripheral retina of *Rd1* mice and any of the above *E2f*-deficient genotypes. These data encouraged us to ask whether upstream factors involved in the cell cycle regulation cascade may have even greater protective potential.

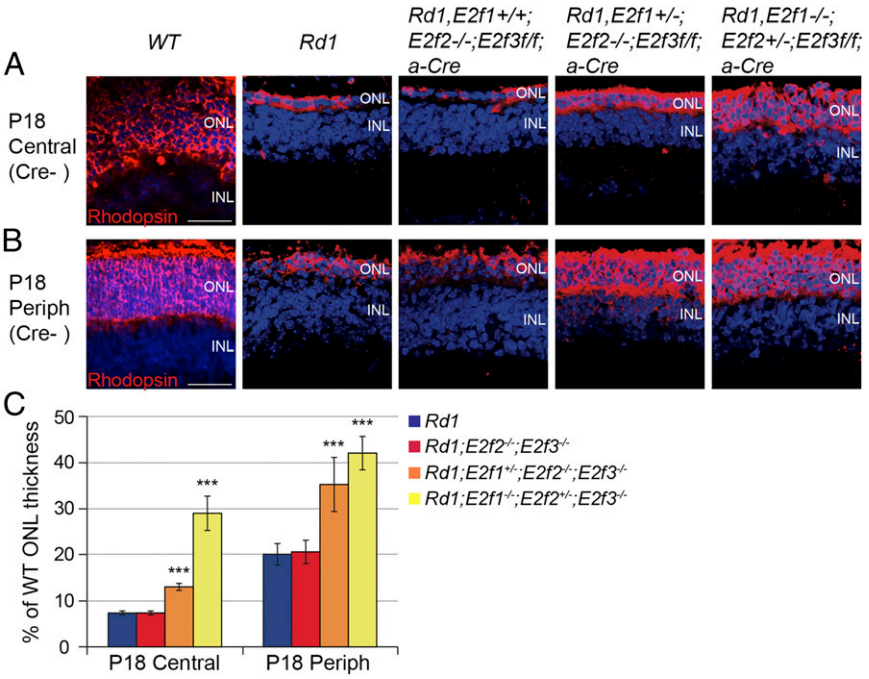

Fig. 2. *E2f1* deletion provides a transient neuroprotection in *Rd1* mice. *A* and *B* depict the rescue of photoreceptors in *Rd1 E2f1* mutants, respectively, in the central and peripheral retina at P18. For the genotypes, refer to figures, main text, and *Materials and Methods*. For quantification, refer to *C*, which presents the photoreceptor row number in percentage of WT values ± SEM ($n = 3$ animals for each genotype, ***$P < 0.001$ compared with *Rd1* and *Rd1;E2f1*$^{+/+}$*;E2f2*$^{-/-}$*;E2f3*$^{f/f}$*;α-Cre*). Note the rescue obtained with *Rd1;E2f1*$^{+/-}$*;E2f2*$^{-/-}$*;E2f3*$^{f/f}$*;α-Cre* and *Rd1;E2f1*$^{-/-}$*;E2f2*$^{+/-}$*;E2f3*$^{f/f}$*;α-Cre* mice. INL, inner nuclear layer; ONL, outer nuclear layer. (Scale bars: 50 μm.)

Extended Protection of Rod Photoreceptors in *Rd1;Bmi1*$^{-/-}$ Mice. Bmi1 promotes cell cycle progression by repressing several tumor suppressor genes, including the CDK4/6 inhibitor *p16*^{Ink4a} (17, 22). We hypothesized that deleting *Bmi1* would reach a broader spectrum of targets than *E2f1* deletion and may thus have a stronger neuroprotective effect. First, we characterized Bmi1 expression at the end of retinal development in WT mice and at early stages of retinal degeneration in *Rd1* mice. Bmi1 was expressed in the nuclei of all cell types of the inner nuclear layer (INL) and ONL, including rods and cones in both WT and *Rd1* retinas at P12 (Fig. 3*A* and Fig. S1). RT-PCR analysis did not reveal any substantial change in the level of *Bmi1* expression between WT and *Rd1* retinas, either at P11 or at P12 (Fig. 3*A*, *Right*). Nevertheless, the presence of Bmi1, which may have several targets (23–26), in the *Rd1* ONL encouraged us to study its potential action. To test the hypothesis that *Bmi1* deletion may limit retinal degeneration, we analyzed the histology of WT, *Rd1*, and *Rd1;Bmi1*$^{-/-}$ retinas at early (P12), middle (P15 and P18), and late (P30 and P34) stages of the disease (Fig. 3*B*). Removing only one *Bmi1* allele in *Rd1;Bmi1*$^{+/-}$ retinas did not induce any change in the progression of retinal degeneration (Fig. 3*C*). Rhodopsin-stained rod outer segments were similar in *Rd1* and *Rd1;Bmi1*$^{-/-}$ retinas at P12 (Fig. 3*B*). At P15, rhodopsin staining and the thickness of the ONL were already strongly reduced in *Rd1* mice whereas *Rd1;Bmi1*$^{-/-}$ animals displayed an almost normal ONL (Fig. 3*B*). At P18, *Rd1* and *Rd1;Bmi1*$^{-/-}$ retinas harbored 10% and 60% of photoreceptor rows, respectively, compared with WT controls (Fig. 3 *B–D*). At P30, *Rd1;Bmi1*$^{-/-}$ mice still displayed well-preserved rhodopsin-positive outer segments (Fig. 3*B*) and even at P34, they harbored 58.5% of the photoreceptor rows normally present in WT retinas, whereas only a single row of scattered photoreceptors (<10% of a WT retina and consisting mostly of cones) was present in *Rd1* mice (Fig. 3 *B–E*). Analysis of older mice was not possible due to the ataxia and epilepsy characteristic of *Bmi1* null animals. Because loss of rods is followed by slower degeneration of cones, we quantified GNAT2- and S-opsin–positive cone segments at P34. Whereas both markers were already strongly diminished in *Rd1* mice, GNAT2- and S-opsin–positive cells were reduced only by 25% in *Rd1;Bmi1*$^{-/-}$ littermates compared with those in age-matched WT retinas (Fig. 3 *D* and *E*).

These data suggest that removing Bmi1 may have a beneficial effect on the loss of vision. Thus, we next investigated retinal function, by electroretinogram recordings under scotopic conditions (low-intensity light stimuli after dark adaptation, followed by light stimuli at increasing intensities) to determine the minimal intensity of light that is required to elicit a photoreceptor response. *Rd1;Bmi1*$^{-/-}$ mice ranging from age P27 to P30 responded in a dose-dependent manner to increasing light stimuli (Fig. 4*A* shows explanation and Fig. 4 *B–D* and Fig. S4 show results). The response threshold in *Rd1;Bmi1*$^{-/-}$ was situated between a light stimulus of 0.03 and 0.1 cd·s/m^2, which corresponds to the intensity at which cones start to be activated (27). This pattern of response is consistent with the fact that rods are inactive due to the absence of the PDE6β protein essential for the phototransduction, but that their rescue promotes cone survival. Moreover, this response was remarkable in comparison with the almost complete absence of any response in the *Rd1* mouse and is particularly significant compared with previous reports showing only limited rescue of photoreceptors using calcium blockers (3), neurotrophic factors (2), or cell transplantation (28) and gene replacement (29). Insulin treatment of the *Rd1* mouse also increased cone survival, but to a lesser extent (30). Their function has not been investigated in this study. Although we cannot exclude the possibility that *Bmi1* deletion directly promotes cone survival in *Rd1;Bmi*$^{-/-}$ mice, this protection is probably due to an indirect effect of rod survival (31). Together, these data show that deletion of *Bmi1* results in a robust neuroprotection to an extent never reached by other neuroprotective approaches (2–4, 31) or by gene therapy (29, 32).

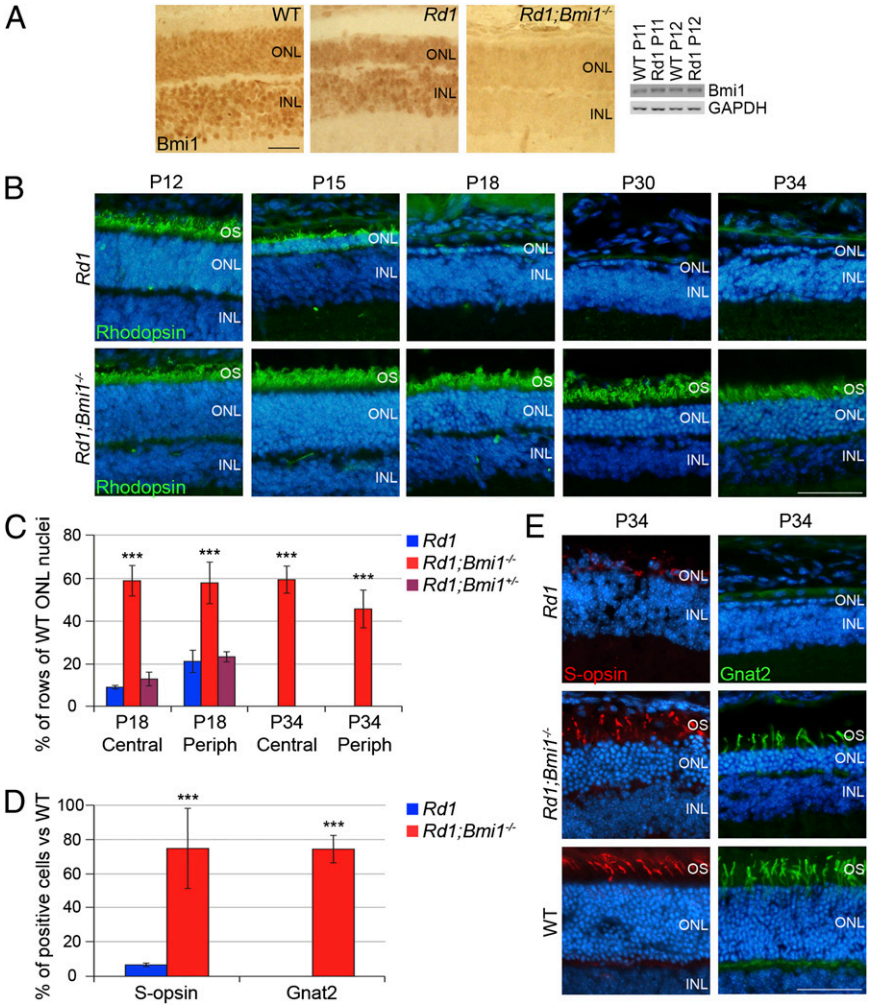

Fig. 3. *Bmi1* deletion delays photoreceptor loss in *Rd1* mice. (*A*) Bmi1 expression (brown) at P12 in WT, *Rd1*, and *Rd1;Bmi1*$^{-/-}$ (negative control) retinas. (*Right*) Confirmation of this expression by RT-PCR of total mRNA extracts of P11 and P12 retinas. (*B*) The thickness of the ONL and rhodopsin staining (green) decrease rapidly in *Rd1* mice. P30 *Rd1* retinas harbor only a single scattered row of photoreceptors. By contrast, numerous rhodopsin-expressing photoreceptors are present between P12 and P34 in the *Rd1;Bmi1*$^{-/-}$ retinas. Note the large band of photoreceptor outer segment (OS). (*C*) Quantification of the number of rows of photoreceptor nuclei in *Rd1* and *Rd1;Bmi1*$^{-/-}$ mice at P18 and P34 vs. those in age-matched WT retinas. (*D*) Quantification of cones expressing S-opsin and GNAT2 in P34 Rd1 retina compared with those in age-matched WT controls. (*C* and *D*) All data are expressed as percentages compared with those in age-matched WT retinas ± SEM (n = 3 animals for each genotype). ***$P < 0.001$ between *Rd1* and *Rd1;Bmi1*$^{-/-}$. (*E*) S-opsin and GNAT2 expression in cone outer segments of *Rd1*, *Rd1;Bmi1*$^{-/-}$, and WT retinas at P34. INL, inner nuclear layer; ONL, outer nuclear layer; OS, outer segments. (Scale bars: 50 μm.)

***Bmi1* Regulates Cell Cycle Proteins in the Degenerating Retina.** One of the best known roles of *Bmi1* is to support cell cycle progression by promoting CDK activity during the G1 phase and at the G1/S checkpoint. Therefore, we analyzed cell cycle markers in *Rd1;Bmi1*$^{-/-}$ mice at P12 and compared them to those in the WT and *Rd1* littermates mentioned above. Deletion of *Bmi1* decreased the amount of CDK4-positive photoreceptors by 46% compared with that in *Rd1* mice (Fig. 5 *A* and *B*). Fewer CDK2-positive photoreceptor nuclei were found in *Rd1;Bmi1*$^{-/-}$ retinas in comparison with those of *Rd1*. Very few CDK2-positive cells were observed in *Rd1* and *Rd1;Bmi1*$^{-/-}$ retinas (2 ± 0.9 and 1.1 ± 1 CDK2-positive cells per 100 μm for P12 *Rd1* and *Rd1;Bmi1*$^{-/-}$ retinas, respectively). Consistent with a Bmi1-dependent regulation of cell cycle proteins in the *Rd1* ONL, phosphorylation of Rb on serine 807 and 811 was not detected in *Rd1;Bmi1*$^{-/-}$ photoreceptors at P12.

During the course of retinal degeneration, DNA repair is part of the cascade of events that trigger photoreceptor death (14). In other neurodegenerative diseases, DNA repair is considered to precede the reactivation of CDKs in dying neurons (33). Thus, we analyzed retinas for expression of the DNA repair-specific Ligase IV at P12 and observed similar numbers of sporadic positive photoreceptors in *Rd1* and *Rd1;Bmi1*$^{-/-}$ retinas (Fig. S5). Taken together, these data show that *Bmi1* deletion efficiently reduces retinal degeneration in *Rd1* mice, that its effect likely occurs downstream of DNA repair events, and that it prevents the induction of CDKs and phosphorylation of Rb.

***Ink4a/Arf* Locus Is Not Required to Delay Retinal Degeneration.** The *Ink4a/Arf* locus, encoding the tumor suppressors p16^{Ink4a} and p19^{Arf}, is one of the best known targets of Bmi1 in the regulation of cell cycle and apoptosis. Briefly, p16^{Ink4a} inhibits CDK4/6 activity and its induction in the absence of *Bmi1* (17) could, therefore, mediate protection of *Rd1* photoreceptors. p19^{Arf} stabilizes p53, and although p53 is not required for retinal degeneration in *Rd1* mice (34), p19^{Arf} also has p53-independent effects (35). To determine whether the rescue of retinal degeneration in *Rd1;Bmi1*$^{-/-}$ mice was dependent on p16^{Ink4a} and/

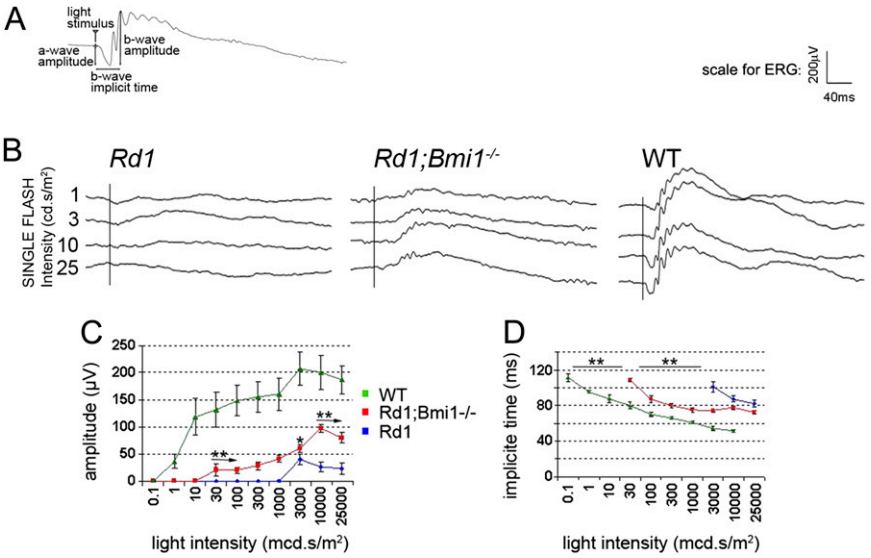

Fig. 4. Rescue of retinal function in *Rd1;Bmi1*$^{-/-}$ mice. (*A*) Schematic representation of a WT ERG response. The a-wave is due to photoreceptor activity, whereas the b-wave is caused by subsequent activation of retinal interneurons. (*Right*) Scale bars for amplitude (μV) and implicit time (ms) are shown. (*B*) Representative ERG recordings of *Rd1*, *Rd1;Bmi1*$^{-/-}$, and WT mice at P27–P30 in scotopic conditions at high light intensities. Refer to Fig. S4 for complete ERG curves. Quantification is shown for the b-wave amplitude (*C*) and the implicit time (delay of the response) of the b-wave (*D*). $*P < 0.05$, $**P < 0.01$ between *Rd1* and *Rd1;Bmi1*$^{-/-}$.

or p19^{Arf}, we analyzed *Rd1;Bmi1*$^{-/-}$*;Ink4a/Arf*$^{-/-}$ triple null mice at ages P18 (Fig. 5*C*) and P34 (Fig. 5*D*) and quantified the number of photoreceptor rows (Fig. 5*E*) in the peripheral and in the central retina. Surprisingly, we did not observe any difference between *Rd1;Bmi1*$^{-/-}$ and *Rd1;Bmi1*$^{-/-}$*;Ink4a/Arf*$^{-/-}$ mice (Fig. 5), suggesting that *Bmi1* loss delays retinal degeneration and down-regulates CDK expression in *Rd1* mice in a process that is *Ink4a/Arf* independent.

Discussion

Previous work has implicated the reactivation of cell cycle components as a key feature of neurodegenerative diseases. The relevance of this mechanism in photoreceptor degeneration was unclear and the role of Bmi1 had never been investigated in any neurodegenerative disease. Here, we show that nuclear expression of CDK4, CDK6, and CDK2 and phosphorylation of Rb precede photoreceptor death in models of retinal degeneration. Roscovitine treatment of *Rd1* retinal explants decreased photoreceptor death, supporting the relevance of a relationship between CDK activation and cell death. Deleting *E2f*s (mainly *E2f1*) on the *Rd1* background resulted in a transient neuroprotection, whereas deletion of *Bmi1* (upstream of E2F1 and CDKs) led to an extensive delay in photoreceptor loss. Mortality at 5–6 wk precludes the determination of the full protective extent of *Bmi1* deletion. The future availability of conditional knockouts or knockdown approaches may reveal the full extent of photoreceptor survival conferred by Bmi1 depletion and whether Müller cells play a certain function (protection, cell replacement). In other neurodegenerative diseases, severe DNA damage is a major signal to induce cell death and is considered to be upstream of CDK expression (36). The presence of Ligase IV in *Rd1* mouse retina (this paper and ref. 14) at early stages of the degeneration process also suggests a similar phenomenon for the retina. The presence of Ligase IV in *Rd1;Bmi1*$^{-/-}$ retina suggests that the neuroprotective effect of *Bmi1* deletion occurs downstream of DNA repair, via CDK inactivation. Nonetheless, we cannot exclude a modest effect of *Bmi1* deletion on DNA repair, because Bmi1 has been reported to be involved in DNA repair initiation (37, 38). In contrast, there is recent evidence that *Bmi1* loss increases oxidative stress in neurons (39) as well as in other cell types (40). In consequence, our results show that *Bmi1* deletion can have a dual effect on cell survival, making investigations on the direct and indirect Bmi1 targets a priority for future studies, to generate appropriate tools for therapy. Other known epigenetic regulators were recently shown to control photoreceptor survival in *Rd1* retina explants, such as histone deacetylase 4 (HDAC4) (41), as well as photoreceptor death, such as unidentified members of the HDAC classes I and II, as revealed by the nonspecific inhibitor trichostatin (42). However, no direct evidence on epigenetic modification has been gathered so far. Moreover, HDAC4 survival action occurs in the cytoplasm through hyopxia-inducible factor 1 (HIF1) stabilization (41), revealing the different action modes of HDACs. Binding of the Bmi1-containing polycomb-repressing complex to DNA requires histone deacetylation and Histone-3 methylation. Analyzing these epigenetic regulators in the cytoplasm and nucleus, as well as modifications in *Rd1* and *Rd1;Bmi1*$^{-/-}$ retinas, will help to identify important targets that mediate photoreceptor death.

We have now implicated several cell cycle regulators in photoreceptor death. The broader effect of *Bmi1* deletion compared with *Rd1;E2f1*$^{-/-}$ may be explained by its position upstream of E2F1 and its regulatory action on a large panel of tumor suppressors and CDKs. The wide spectrum of targets for Bmi1 and polycomb complexes (23–26) may also clarify why the photoreceptor rescue observed in *Rd1;Bmi1*$^{-/-}$ mice does not depend exclusively on the *Ink4a/Arf* locus. The use of the Cre system to specifically delete E2Fs in photoreceptors, the observation of photoreceptor survival after the inhibition of CDK expression or activity, either by Bmi1 loss or roscovitine treatment, and the variation of Rb phosphorylation paralleling CDK expression imply the cell-intrinsic importance of cell cycle protein reactivation in the control of photoreceptor death. Although we cannot exclude that the survival effect mediated by Bmi1 deletion may also be partially attributed to other retinal cell types, such as Müller glia, our results highlight the role of Bmi1 in the regulation of cell cycle proteins during the cell death process in an animal model of retinal degeneration. In the retina, Müller cells support photoreceptors by regulating their metabolism and through neurotrophic factor delivery (43). However, such neurotrophic factors had only mild neuroprotective effects that are

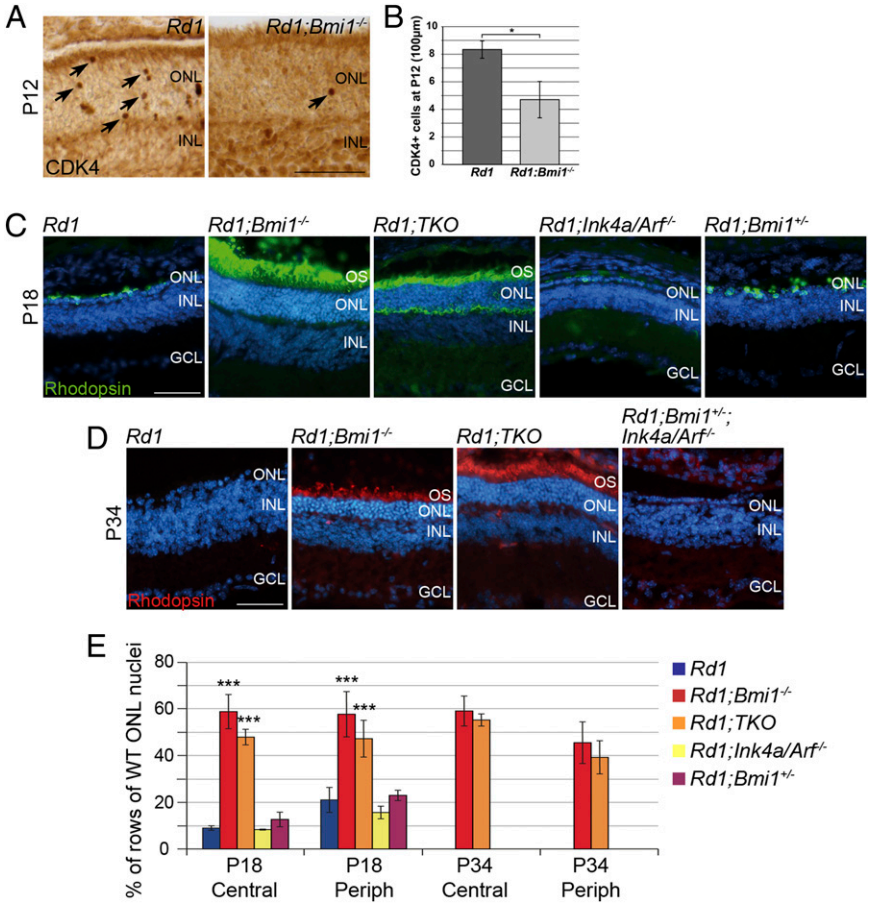

Fig. 5. *Bmi1* loss acts on the *Rd1* photoreceptor rescue independently on the *Ink4a/Arf* locus and by decreasing Cdk4 expression. (*A*) CDK4 (brown spots and arrows) stainings in the P12 *Rd1* and *Rd1;Bmi1*$^{-/-}$ retina. (*B*) Quantification of CDK4-positive photoreceptors in *Rd1* and *Rd1;Bmi1*$^{-/-}$ retinas, values ± SEM (n = 3 animals for each genotype). *$P < 0.05$. (*C* and *D*) Amount of photoreceptors present at P18 and P34, respectively, in different genetic models. (*C*) Whereas the *Rd1* retina shows one to two rows of photoreceptors positive for rhodopsin (green), the deletion of *Bmi1* rescues these cells markedly. The ablation of *Inka4/Arf* does not reverse the rescue induced by *Bmi1* deletion (*Rd1*;TKO, *Rd1*;triple knockout) nor does it affect the process of retinal degeneration (*Rd1;Ink4a/Arf*$^{-/-}$). Bmi1 has no dose effect to prevent retinal degeneration (*Rd1;Bmi1*$^{+/-}$). (*D*) At P34 the rescue is still robust both in *Rd1;Bmi1*$^{-/-}$ and in *Rd1*;TKO, which shows similar rescue. The presence of one *Bmi1* allele in *Rd1;Ink4a/Arf*$^{-/-}$ is sufficient to sustain retinal degeneration. For quantification, refer to *E*, which presents the photoreceptor row number in percentage of the WT values ± SEM (n = 3 animals for each genotype). ***$P < 0.001$ compared with *Rd1*, *Rd1;Ink4a/Arf*$^{-/-}$, and *Rd1;Bmi1*$^{+/-}$. GCL, ganglion cell layer; INL, inner nuclear layer; ONL, outer nuclear layer; OS, outer segments. (Scale bar: 50 μm.)

not comparable to the Bmi1 loss-mediated delay of retinal degeneration. In consequence in *Rd1;Bmi1*$^{-/-}$ retina, a potential role in neurotrophic support by glial cells is probably minor.

A recent report revealed that cGMP is an important mediator during the early phases of photoreceptor death (5). Indeed, deletion of the *Cngb1* gene coding for a channel regulated by cGMP strongly delayed photoreceptor death in *Rd1* mice. Around 50% of the photoreceptor cells survived at P30 and 39% at P60. The relationship between Bmi1 and cGMP remains to be identified and may reveal important mechanisms controlling sensory neuron death.

Our results with the *Rd1* model of RP raise the possibility that the *Bmi1*-dependent reactivation of cell cycle components may be relevant to a much wider range of retinopathies. Indeed, we also detected CDK4 and CDK2 reactivation coincident with light damage-induced retinal degeneration and other recessive and dominant rodent models of retinal dystrophies. The relevance of *Bmi1* in neurodegeneration is unique and should be investigated in other models of retinal degeneration, such as light-induced damage, as well as in other CNS conditions where a cell cycle-related mechanism has already been implicated in apoptosis (10). Indeed, a small neuroprotective effect (*E2f1* deletion, CDK inhibition) measured in the rapidly degenerating *Rd1* model would likely translate into considerable therapeutic benefit in humans where photoreceptor loss occurs over years rather than days. These results, coupled with the CDK analyses above, provide two promising targets for therapeutic intervention in patients with RP and show clearly that reactivated cell cycle components contribute to the demise of photoreceptors. Interestingly, in the adult cerebral cortex and cerebellum, Bmi1 is expressed at low levels by virtually all neurons (44), supporting a potential broad role for this Polycomb repressor in controlling neuronal cell death. The *Bmi1* pathway thus merits being studied in different forms of retinal degeneration and neurodegenerative diseases.

Materials and Methods

Animals and Genotypes. *Rd1*, *Rd1;Bmi1*$^{-/-}$, and *Rd1;Bmi1*$^{-/-}$*;Ink4a/Arf*$^{-/-}$ (*Rd1;TKO*) mice on a FVB background were maintained and genotyped by standard PCR as previously described (17, 22, 45). For production of *Rd1;Bmi1*$^{-/-}$, *Rd1;Bmi*$^{+/-}$ breeders were used because homozygotes are viable until around P30 only. *Rd1;TKO* mice were generated by crossing *Bmi1*$^{+/-}$ and *Ink4a/Arf*$^{-/-}$ mice (46), both having an FVB (*Rd1*) genetic background. To assess the role of E2F factors in *Rd1* mice, *E2f1* and *E2f2* mutants on the FVB background, as well as FVB mice carrying a *E2f3* floxed allele (15), were interbred with *a-Cre* mice (P. Gruss, Göttingen, Germany) to obtain the following genotypes: *Rd1;E2f2*$^{-/-}$*;E2f3*$^{-/-}$, *Rd1;E2f1*$^{+/-}$*;E2f2*$^{-/-}$*;E2f3*$^{-/-}$, and

Rd1;E2f1$^{-/-}$;*E2f2*$^{+/-}$;*E2f3*$^{-/-}$. Note that the α-promoter was active only in the peripheral retina, keeping therefore the central retina wild type for *E2f3*. FVB.129P2;*Pde6b*$^{+}$ mice obtained from Charles River Laboratories (stock no. 004828) were used as WT sighted controls. Mice were treated according to institutional and national as well as the Association for Research in Vision and Ophthalmology (ARVO) guidelines, and all experimental procedures were approved by national veterinary authorities.

Histological Analysis and Quantification. Histological analysis of WT, *Rd1*, and *Rd1;Bmi1*$^{-/-}$ mutants was performed at P9, P11, P12, P15, P18, P30, and P34. *Rd1;E2f* mutants were analyzed at P18 and P26. Upon enucleation, eye globes were fixed for 1 h in 4% (wt/vol) paraformaldehyde (PFA) and then transferred either to 25% (wt/vol) sucrose to obtain 14-μm-thick cryosections, or to PBS before being mounted in paraffin and cut into 5-μm-thick sections. Before being processed at the cryostat, the eyes were oriented to allow the discrimination between dorsal and ventral retina. The sections were collected on six serial slides for each eye, allowing multiple labeling throughout the entire eye for each slide. All measurements were performed on the two most central cryosections including (or surrounding) the optic nerve. Measurements of rows of nuclei were taken at 150 and 250 μm from the periphery of the retina at both dorsal and ventral extremities and data were pooled as a mean for the peripheral retina. The measurements for the central retina are the mean of the data obtained at 300 and 400 μm dorsally and ventrally from the optic nerve head. The measures were taken using an Olympus BX60 fluorescence microscope and the AnalySIS 3.0 software (Soft Imaging) for *Bmi1* and *Ink4a/Arf* mutants, whereas *E2f* mutant retinas were analyzed with a Zeiss Axioplan-2 microscope and the Axiovision 4.0 software.

Immunohistochemistry and Antibodies. Immunohistochemical analysis was performed on either cryostat sections or paraffin sections of the whole eyecup. All primary antibodies, their source, and their working dilutions for frozen and/or paraffin sections are listed in Table S1. The standard protocol used for immunochemistry on cryostat sections included 1 h of blocking with 10% (vol/vol) normal goat serum and 0.3% (wt/vol) TritonX; followed by overnight incubation with the primary antibody diluted in blocking solution; and finally revelation with the appropriate Alexa 633, Alexa 488, FITC, or Cy3-coupled secondary antibody (details in Table S2). All exceptions to the standard protocol are noted in Table S1. In certain cases, as specified in Table S1, the TSA Amplification System (PerkinElmer) was used to enhance the fluorescent signal in accordance to manufacturer's protocol. For stainings on paraffin sections, after the hydration steps, the sections were microwave boiled in a retrieving citrate buffer for 1 min at 900 W and 15 min at 250 W. Endogenous peroxidases were quenched with a 30-min treatment with 3% (vol/vol) H_2O_2. Primary antibodies were added overnight in 1% (wt/vol) BSA in PBS, and stainings were visualized using the appropriate biotinylated antibody (Table S2) with the Vectastain ABC Kit (Vector) according to the manufacturer's protocol. On both frozen and cryostat sections, the nuclei were counterstained with 4′,6-diamidino-2-phenylindole (DAPI). All measurements were taken using an Olympus BX60 fluorescence microscope and the AnalySIS 3.0 software (Soft Imaging). Quantifications of positive cells were performed on pictures of central retina (450-μm length) and normalized to 100 μm. When specified in the figure legends, confocal analysis was performed using a Zeiss öS; 510 Meta confocal microscope and the Zeiss LSM 510 3.2 software.

EdU Injection and Detection. To reveal DNA synthesis in *Rd1* mice, anti-EdU staining was performed on retinal frozen sections from P12 *Rd1* mice that had received i.p. injections of EdU (40 μg/g body weight; Click-iT Edu Imaging Kit, Invitrogen) 24 h earlier.

Retinal Explant Cultures. Retinal explants were cultured in R-16 medium (47, 48) (Gibco). The complete R-16 medium is prepared by adding 19 supplements (all purchased from Sigma), composed of BSA, hormones, and vitamins, to the stock solution (details in ref. 49). In our experimental paradigm, retinal explants generated from P6 *Rd1* mice were cultured in complete R-16 medium for 6 d. One day later (P6 + 1 DIV) the medium was changed, and the explants were cultured either in R-16 medium containing 50 μM Roscovitine (Sigma) resuspended in 50:50 PBS/DMSO or in R-16-medium with 0.125% DMSO. Subsequently, the medium (with or without Roscovitine) was replenished every second day. The explants were fixed at P6 + 6 DIV with 4% PFA for 2 h at RT, before being transferred to 10% and 25% sucrose (in PBS). Each explant was processed into 10 series of 12-μm cryosections. TUNEL-positive cells were counted on the most central sections and normalized to the length of the explant.

Electroretinograms. The procedure for electroretinogram (ERG) recordings is fully described in a previous study (50). Briefly, the mice were dark adapted overnight and anesthetized by an i.p. injection of a mixture of ketamine (100 mg/kg) and xylazine (15 mg/kg), and pupils were dilated. ERG recordings were obtained using a Ganzfeld stimulator from a Multiliner Vision apparatus (Jaeger/Tonnies) under dark-adapted (scotopic) conditions. The ERG was recorded in response to single flashes of white light of the following increasing intensities: 1×10^{-4}, 1×10^{-3}, 1×10^{-2}, 3×10^{-2}, 1×10^{-1}, 3×10^{-1}, 1, 3, 10, and 25 cd·s/m^2 to determine at which intensity of light the retina is active. For each intensity, 10–30 responses were averaged. Band-pass filter cutoff frequencies were 0.3 and 300 Hz. The a-wave amplitude corresponds to photoreceptor activity and is the negative shape of the curve (Fig. 4). The b-wave amplitude was defined as the difference between b-wave and a-wave peaks (or the baseline level when the a-wave was not detectable) and corresponds to the interneuron signals stimulated by the photoreceptors. Amplitudes are expressed in microvolts and latencies in milliseconds.

RNA Extraction and RT-PCR. Four P12 WT or *Rd1* retinas were triturated with ophthalmic scissors, pooled, homogenized in 1 mL of Tri Reagent (Sigma), processed according to the manufacturer's datasheet, and subsequently resuspended in 20 μL of RNase-free water. Samples were treated with a DNase Kit (Ambion; 1906) as described on the datasheet. Reverse transcription was performed as previously described. PCRs for *Bmi1* and *Gapdh* were performed using the following primers at a final concentration of 0.2 μM each: *Bmi1*-F, 5′CAGCAATGACTGTGATGC3′; *Bmi1*-R, 5′CTCCAGCATTCGTCAGTC3′; *Gapdh*-F, 5′ACCACAGTCCATGCCATCAC3′; and *Gapdh*-R, 5′TCCACCACCCTGTTGCTGTA3′, using a standard Taq Polymerase (Invitrogen) and 2 mM $MgCl_2$. Non–reverse-transcribed samples were used to check for genomic DNA contamination. Amplifications were carried out under the following conditions: denaturation for 5 min at 94 °C; followed by 34 cycles of denaturation at 94 °C for 30 s, annealing for 60 s at 52 °C (for *Bmi1*) or 62 °C (for *Gapdh*), and extension at 72 °C for 60 s; with a final extension at 72 °C for 10 min. PCR products were visualized using 1.5% agarose gels with SYBRsafe (Invitrogen; diluted 1/10,000).

Light Damage. Eight-week-old BALB-C mice (Charles River) were kept for 3 wk in cyclic light at or below 80 lux (lx). After being dark adapted overnight, mice were exposed to 5,000 lx (measured on the cage floor) of white fluorescent light in reflective cages for 1 h. In these series of experiments, the eyes were enucleated for histological analysis after 36 h of recovery time in the dark.

Statistical Analysis. One-way ANOVA followed by a Bonferroni test was applied to data, which were considered statistically different with a $P < 0.05$. When only two groups were compared, an impaired two-tailed *t* test was applied to data, and a $P < 0.05$ implied statistical significance. A minimum of three animals were analyzed for each histological quantification, and a minimum of six eyes were considered for ERG analysis.

ACKNOWLEDGMENTS. We thank François Paquet-Durand for providing retina slices of P23H and *S334ter* rats; Dana Wanner and Meriem Tekaya for their excellent technical support; and Sophia Bruggeman, Corinne Kostic, and Francis Munier for rich discussions. This work was supported by Swiss National Foundation Grant 31000A0-122321 and by the AAVEYE (FP7-223445) consortium.

1. Hartong DT, Berson EL, Dryja TP (2006) Retinitis pigmentosa. *Lancet* 368(9549): 1795–1809.
2. LaVail MM, et al. (1998) Protection of mouse photoreceptors by survival factors in retinal degenerations. *Invest Ophthalmol Vis Sci* 39(3):592–602.
3. Frasson M, et al. (1999) Retinitis pigmentosa: Rod photoreceptor rescue by a calcium-channel blocker in the rd mouse. *Nat Med* 5(10):1183–1187.
4. Bennett J, et al. (1998) Adenovirus-mediated delivery of rhodopsin-promoted bcl-2 results in a delay in photoreceptor cell death in the rd/rd mouse. *Gene Ther* 5(9):1156–1164.
5. Paquet-Durand F, et al. (2011) A key role for cyclic nucleotide gated (CNG) channels in cGMP-related retinitis pigmentosa. *Hum Mol Genet* 20(5):941–947.
6. Vincent I, Rosado M, Davies P (1996) Mitotic mechanisms in Alzheimer's disease? *J Cell Biol* 132(3):413–425.
7. Yang Y, Geldmacher DS, Herrup K (2001) DNA replication precedes neuronal cell death in Alzheimer's disease. *J Neurosci* 21(8):2661–2668.
8. Höglinger GU, et al. (2007) The pRb/E2F cell-cycle pathway mediates cell death in Parkinson's disease. *Proc Natl Acad Sci USA* 104(9):3585–3590.

9. Nguyen MD, et al. (2003) Cell cycle regulators in the neuronal death pathway of amyotrophic lateral sclerosis caused by mutant superoxide dismutase 1. *J Neurosci* 23(6):2131–2140.
10. Herrup K, Yang Y (2007) Cell cycle regulation in the postmitotic neuron: Oxymoron or new biology? *Nat Rev Neurosci* 8(5):368–378.
11. Appert-Collin A, et al. (2006) Cyclin dependent kinase inhibitors prevent apoptosis of postmitotic mouse motoneurons. *Life Sci* 79(5):484–490.
12. Park DS, Levine B, Ferrari G, Greene LA (1997) Cyclin dependent kinase inhibitors and dominant negative cyclin dependent kinase 4 and 6 promote survival of NGF-deprived sympathetic neurons. *J Neurosci* 17(23):8975–8983.
13. Osuga H, et al. (2000) Cyclin-dependent kinases as a therapeutic target for stroke. *Proc Natl Acad Sci USA* 97(18):10254–10259.
14. Menu dit Huart L, Lorentz O, Goureau O, Leveillard T, Sahel JA (2004) DNA repair in the degenerating mouse retina. *Mol Cell Neurosci* 26(3):441–449.
15. Chen D, et al. (2007) Rb-mediated neuronal differentiation through cell-cycle-independent regulation of E2f3a. *PLoS Biol* 5(7):e179.
16. Sharpless NE, DePinho RA (1999) The INK4A/ARF locus and its two gene products. *Curr Opin Genet Dev* 9(1):22–30.
17. Jacobs JJ, Kieboom K, Marino S, DePinho RA, van Lohuizen M (1999) The oncogene and Polycomb-group gene bmi-1 regulates cell proliferation and senescence through the ink4a locus. *Nature* 397(6715):164–168.
18. Wenzel A, Grimm C, Samardzija M, Remé CE (2005) Molecular mechanisms of light-induced photoreceptor apoptosis and neuroprotection for retinal degeneration. *Prog Retin Eye Res* 24(2):275–306.
19. Lin SC, Skapek SX, Papermaster DS, Hankin M, Lee EY (2001) The proliferative and apoptotic activities of E2F1 in the mouse retina. *Oncogene* 20(48):7073–7084.
20. Wu L, et al. (2001) The E2F1-3 transcription factors are essential for cellular proliferation. *Nature* 414(6862):457–462.
21. Chen D, et al. (2009) Division and apoptosis of E2f-deficient retinal progenitors. *Nature* 462(7275):925–929.
22. Bruggeman SW, et al. (2005) Ink4a and Arf differentially affect cell proliferation and neural stem cell self-renewal in Bmi1-deficient mice. *Genes Dev* 19(12):1438–1443.
23. Boyer LA, et al. (2006) Polycomb complexes repress developmental regulators in murine embryonic stem cells. *Nature* 441(7091):349–353.
24. Kallin EM, et al. (2009) Genome-wide uH2A localization analysis highlights Bmi1-dependent deposition of the mark at repressed genes. *PLoS Genet* 5(6):e1000506.
25. Meng S, et al. (2010) Identification and characterization of Bmi-1-responding element within the human p16 promoter. *J Biol Chem* 285(43):33219–33229.
26. Tolhuis B, et al. (2006) Genome-wide profiling of PRC1 and PRC2 Polycomb chromatin binding in Drosophila melanogaster. *Nat Genet* 38(6):694–699.
27. Seeliger MW, et al. (2001) New views on RPE65 deficiency: The rod system is the source of vision in a mouse model of Leber congenital amaurosis. *Nat Genet* 29(1): 70–74.
28. Otani A, et al. (2002) Bone marrow-derived stem cells target retinal astrocytes and can promote or inhibit retinal angiogenesis. *Nat Med* 8(9):1004–1010.
29. Bennett J, et al. (1996) Photoreceptor cell rescue in retinal degeneration (rd) mice by in vivo gene therapy. *Nat Med* 2(6):649–654.
30. Punzo C, Kornacker K, Cepko CL (2009) Stimulation of the insulin/mTOR pathway delays cone death in a mouse model of retinitis pigmentosa. *Nat Neurosci* 12(1): 44–52.
31. Léveillard T, et al. (2004) Identification and characterization of rod-derived cone viability factor. *Nat Genet* 36(7):755–759.
32. Takahashi M, Miyoshi H, Verma IM, Gage FH (1999) Rescue from photoreceptor degeneration in the rd mouse by human immunodeficiency virus vector-mediated gene transfer. *J Virol* 73(9):7812–7816.
33. Park DS, et al. (2000) Involvement of retinoblastoma family members and E2F/DP complexes in the death of neurons evoked by DNA damage. *J Neurosci* 20(9): 3104–3114.
34. Wu J, Trogadis J, Bremner R (2001) Rod and cone degeneration in the rd mouse is p53 independent. *Mol Vis* 7:101–106.
35. Sherr CJ (2006) Divorcing ARF and p53: An unsettled case. *Nat Rev Cancer* 6(9): 663–673.
36. Morris EJ, et al. (2001) Cyclin-dependent kinases and P53 pathways are activated independently and mediate Bax activation in neurons after DNA damage. *J Neurosci* 21(14):5017–5026.
37. Facchino S, Abdouh M, Chatoo W, Bernier G (2010) BMI1 confers radioresistance to normal and cancerous neural stem cells through recruitment of the DNA damage response machinery. *J Neurosci* 30(30):10096–10111.
38. Ismail IH, Andrin C, McDonald D, Hendzel MJ (2010) BMI1-mediated histone ubiquitylation promotes DNA double-strand break repair. *J Cell Biol* 191(1):45–60.
39. Chatoo W, et al. (2009) The polycomb group gene Bmi1 regulates antioxidant defenses in neurons by repressing p53 pro-oxidant activity. *J Neurosci* 29(2):529–542.
40. Liu J, et al. (2009) Bmi1 regulates mitochondrial function and the DNA damage response pathway. *Nature* 459(7245):387–392.
41. Chen B, Cepko CL (2009) HDAC4 regulates neuronal survival in normal and diseased retinas. *Science* 323(5911):256–259.
42. Sancho-Pelluz J, et al. (2010) Excessive HDAC activation is critical for neurodegeneration in the rd1 mouse. *Cell Death Dis* 1:e24.
43. Bringmann A, et al. (2009) Cellular signaling and factors involved in Müller cell gliosis: Neuroprotective and detrimental effects. *Prog Retin Eye Res* 28(6):423–451.
44. Bruggeman SW, et al. (2007) Bmi1 controls tumor development in an Ink4a/Arf-independent manner in a mouse model for glioma. *Cancer Cell* 12(4):328–341.
45. van der Lugt NM, et al. (1994) Posterior transformation, neurological abnormalities, and severe hematopoietic defects in mice with a targeted deletion of the bmi-1 proto-oncogene. *Genes Dev* 8(7):757–769.
46. Serrano M, et al. (1996) Role of the INK4a locus in tumor suppression and cell mortality. *Cell* 85(1):27–37.
47. Romijn HJ (1988) Development and advantages of serum-free, chemically defined nutrient media for culturing of nerve tissue. *Biol Cell* 63(3):263–268.
48. Romijn HJ, de Jong BM, Ruijter JM (1988) A procedure for culturing rat neocortex explants in a serum-free nutrient medium. *J Neurosci Methods* 23(1):75–83.
49. Caffé AR, et al. (2001) Mouse retina explants after long-term culture in serum free medium. *J Chem Neuroanat* 22(4):263–273.
50. Bemelmans AP, et al. (2006) Lentiviral gene transfer of RPE65 rescues survival and function of cones in a mouse model of Leber congenital amaurosis. *PLoS Med* 3(10): e347.

Supporting Information

Zencak et al. 10.1073/pnas.1108297110

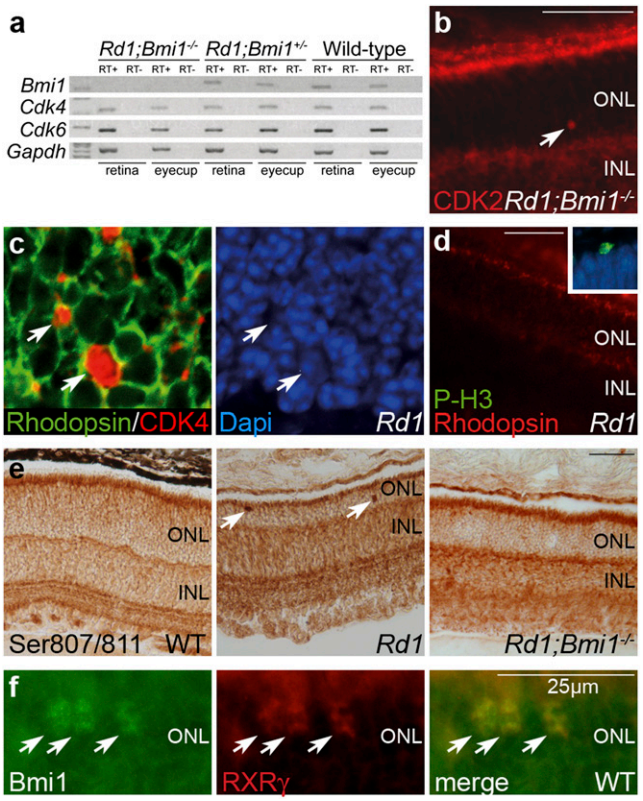

Fig. S1. Expression of cell cycle proteins in P12 retinas. (*A*) RT-PCR analyses of total mRNA extracts from P12 retinas revealed that although WT photoreceptors do not express CDKs (Fig. 1*B*), Bmi1, CDK4, and CDK6 are expressed in WT, *Rd1*, and *Rd1;Bmi1*$^{-/-}$ retinas. (*B*) Few CDK2-positive cells are present in the *Rd1;Bmi1*$^{-/-}$ ONL (arrow). (*C*) High magnification of confocal image confirms that CDK4-expressing cells are Rhodopsin-positive photoreceptors in the *Rd1* ONL. (*D*) The absence of Phospho-H3 in P12 *Rd1* retinas indicates that photoreceptors do not complete the cell cycle. (*Inset*) A cell expressing Phospho-H3 in the newborn retina (positive control). (*E*) Immunohistochemistry against Phospho-Rb Ser807/811 reveals positive cell nuclei in the *Rd1* (*Center*), but not in the WT (*Left*) and in the *Rd1;Bmi1*$^{-/-}$ (*Right*) ONL at P12. Note that a diffuse labeling is present in the outer part of the ONL in all strains. (*F*) Colocalization of Bmi1 (green) with RXRγ (red) reveals that Bmi1 is also present in cone nuclei. (Scale bars in *B* and *D*: 50 μm.)

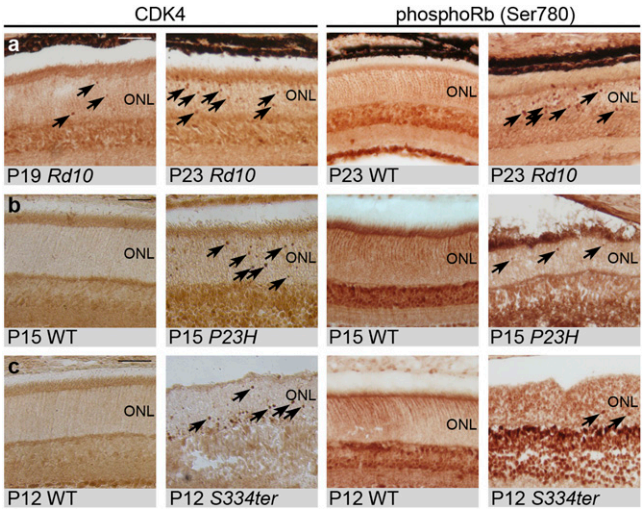

Fig. S2. Photoreceptors express CDK4 and contain phosphorylated retinoblastoma protein (Rb) in several models of retinal degeneration. (*A*) The *Rd10* retina contains CDK4-expressing cells in the ONL (brown nuclei highlighted by arrows) at P19 and P23, when the thickness of the ONL is reduced. At the same time (P23), Rb protein is phosphorylated on serine 780 (Ser780) in the *Rd10* retina, although not detected in the WT ONL nuclei. (*B*) At P15, several photoreceptor nuclei in the *P23H* rat retina are Cdk4 positive and contain phosphorylated Rb on Ser780 (brown, arrows). Such cells are not detected in the WT ONL. (*C*) P12 *S334ter* retinas present CDK4-positive and phosphorylated Rb-positive nuclei (brown) in the ONL, which are absent in P12 WT controls. Arrows point to some representative cells positive for CDK4 and phosphorylated Rb. (Scale bar, 50 μm.)

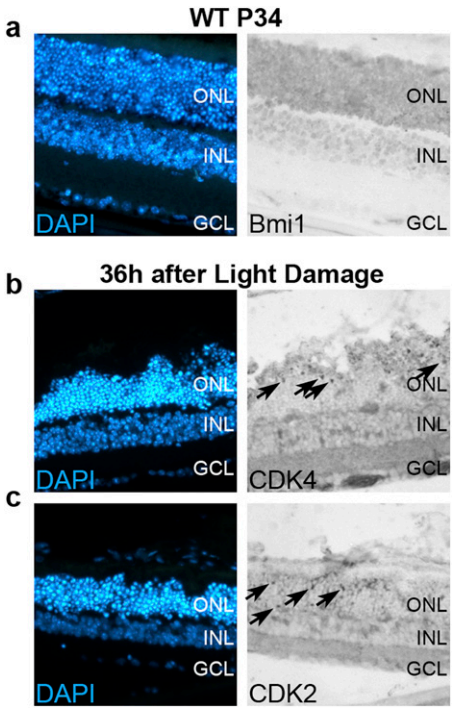

Fig. S3. Cell cycle proteins are expressed during light damage-induced photoreceptor death. (*A*) In the adult WT retina, at P34, Bmi1 is expressed with a similar pattern to that in P12 retinas (Fig. 3). Nearly all INL and ONL nuclei are positive for Bmi1. *Left*, DAPI staining; *Right*, Bmi1 expression (gray). (*B*) Thirty-six hours after light damage, Cdk4 (*Right*, dark gray, arrows) is strongly expressed in injured retinas. CDK4-positive cells are absent from control ONL (no light damage). (*C*) In parallel with CDK4, CDK2 (*Right*, dark gray) is also intensely expressed in light-damaged retinas 36 h after injury, although absent in the control. (Scale bar, 50 μm.)

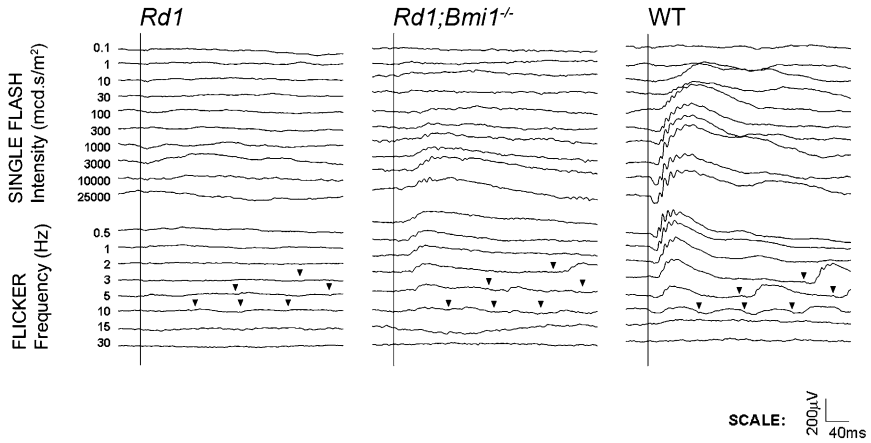

Fig. S4. Assessment of retinal function by scotopic ERG. (*Left* to *Right*) Full scotopic ERG recordings are depicted for *Rd1*, *Rd1;Bmi1*$^{-/-}$, and WT mice. Note that *Rd1* retinas show no response whereas those of *Rd1;Bmi1*$^{-/-}$ mice respond to mild to bright light stimuli, but to a lower extent than WT retinas. *Rd1;Bmi1*$^{-/-}$ mice respond to repeated stimulations (flicker), suggesting that chromophore regeneration occurs normally or that the rescued cone photoreceptors function correctly. Arrowheads in the flicker response point at light stimuli when a response was observed. Note the delayed response in these animals.

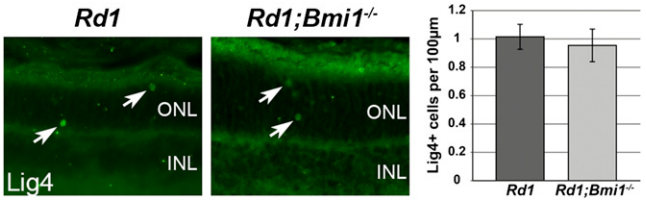

Fig. S5. Both *Rd1* and *Rd1;Bmi1*$^{-/-}$ retinas strongly express DNA damage-specific Ligase IV (Lig4) at P12. (*Left* and *Center*) Lig4 expression in P12 *Rd1* and *Rd1;Bmi1*$^{-/-}$ retinas. Note the staining observed in the ONL of both genotypes (arrows). (Scale bar, 50 µm.) (*Right*) Quantification reveals that the deletion of *Bmi1* in the *Rd1* mouse does not influence the number of Lig4-positive cells in the ONL.

Table S1. Antibody list for immunohistochemistry

Antibody	Species	Source	Working dilution*	Notes
Bmi1 F6	Mouse	M. Van Lohuizen, Netherlands Cancer Institute, Amsterdam	F: 1/50	
Cdk2 (H-298)	Rabbit	Santa Cruz; SC-748	P: 1/200 F: 1/100	
Cdk4 (H-22)	Rabbit	Santa Cruz; SC-601	P: 1/200 F: 1/100	†
Cdk6 (H-230)	Rabbit	Santa Cruz; SC-7181	P: 1/200 F: 1/100	
CRALBP	Rabbit	J. Saari, University of Washington, Seattle	F: 1/1000	
CyclinE (C-19)	Rabbit	Santa Cruz; SC-198	P: 1/200	
E2F-1 (H-137)	Rabbit	Santa Cruz; SC-22820	P: 1/100	
$G_{\alpha}t2$ (=GNAT2)	Rabbit	Santa Cruz; SC-390	F: 1/100	‡
LIG4	Rabbit	Sigma; L5167	F: 1/100	§
M-Opsin	Rabbit	Chemicon; AB 5405	F: 1/1000	¶
p21	Rabbit	Abcam; AB 7960	P: 1/200	
Phospho-Histone H3 (ser10)	Rabbit	Upstate; 06-570	F: 1/200	
Phospho-Rb (Ser807/811)	Rabbit	Cell Signaling; 9308	P: 1/200 W: 1/1000	
Recoverin	Rabbit	Chemicon; AB 5585	F: 1/1000	
Rhodopsin Rho 4D2	Mouse	R. Molday, University of British Columbia, Vancouver, BC, Canada	F: 1/50	
S-Opsin sc14363	Goat	Santa Cruz; SC-14363	F: 1/1000	¶

All stainings on paraffin sections were performed as described in *Materials and Methods*. All stainings on frozen sections were performed as described in *Materials and Methods* section, except those noted in footnotes below.

*F, frozen sections; P, paraffin sections; W, Western blot.

†Pretreatment for BrdU staining is described in Materials and Methods.

‡TSA amplification kit was used according to manufacturer's protocol for immunohistochemistry on frozen sections.

§Sections with primary antibody were incubated overnight at room temperature with 2% NGS and 0.2% TritonX (in PBS).

¶Sections were blocked with 10% horse serum (HS) and 0.2% TritonX, and primary antibody was diluted in 2% HS and 0.2% TritonX (in PBS).

Table S2. Secondary antibodies for immunochemistry

Antibody	Source	Working dilution
Alexa Fluor 633 goat anti-mouse IgG	Invitrogen; A21053	1/2,000
Alexa Fluor 633 goat anti-rabbit IgG	Invitrogen; A21072	1/1,000
Alexa Fluor 488 goat anti-rabbit IgG	Invitrogen; A11070	1/2,000
Alexa Fluor 488 goat anti-mouse IgG	Invitrogen; A21121	1/1,000
Alexa Fluor 488 donkey anti-goat IgG	Invitrogen; A11055	1/1,000
FITC goat anti-rabbit IgG	Jackson ImmunoResearch; 111-096-047	1/100
FITC goat anti-mouse IgG	Jackson ImmunoResearch; 115-096-003	1/100
Cy3 goat anti-mouse IgG	Jackson ImmunoResearch; 115-166-003	1/1,000
Cy3 goat anti-rabbit IgG	Jackson ImmunoResearch; 115-166-003	1/1,000
Biotinylated anti-rabbit IgG	Vector Laboratories; BA-1000	1/200
Biotinylated anti-mouse IgG	Vector Laboratories; BA-9200	1/200